A COMPARISON OF CONVENTIONAL CLASSIFICATION METHODS AND A NEW INDICATOR KRIGING BASED METHOD USING HIGH-SPECTRAL RESOLUTION IMAGES (AVIRIS)

FREEK D. VAN DER MEER

International Institute for Aerospace Survey and Earth Sciences (ITC)
Department of Earth Resources Surveys
Research Scientist in Geological Survey
350 Boulevard 1945, P.O. Box 6, 7500 AA, Enschede, The Netherlands.
ISPRS Technical Commission VII

ABSTRACT. High spectral resolution images (AVIRIS) providing detailed information on the surface mineralogy have been used to evaluate a new indicator kriging based classification technique. This technique directly uses spectral information derived from AVIRIS data instead of information from training areas studied in the field. A small study area of an imaging spectrometer data set covering the Cuprite mining district was selected for its known occurrences of both kaolinite and alunite. Three "conventional" classification methods were applied as well as the new indicator kriging based technique and results were evaluated using shape characteristics of the classes and by comparison with local field geologic information. Indicator kriging performed better than the conventional methods. Furthermore, the new indicator kriging based method provides information on the reliability of the classification which is lacking with the conventional methods.

Key Words: Image Classification, Indicator Kriging, AVIRIS, Cuprite Mining District, Nevada

INTRODUCTION

Remote sensing of earth's surface from aircraft and from spacecraft provides information not easily acquired by surface observations. Until recently, the main limitations of remote sensing were that no subsurface information could be obtained and that surface information lacked specification. Conventional scanners (e.g. Landsat MSS and TM, and SPOT) acquire information in a few separate spectral bands of various widths, thus filtering to a large extent the reflectance characteristics of the surface (Goetz & Rowan, 1981). Therefore, new scanner types were developed with high spectral resolution yielding new image processing techniques to cope with the increased amount of data. The use of indicator kriging as classification routine is discussed in this paper using high spectral resolution imagery although the technique is also valid for conventional scanner data.

IMAGING SPECTROMETRY

The use of high spectral resolution remotely sensed imagery for mineralogic mapping was first demonstrated in spectral laboratory studies (e.g. Hunt, 1977). In 1981, airborne spectrometer data were acquired using a sensor developed by the GER corporation for one-dimensional profiling along a flight line. The first imaging device was the Airborne Imaging Spectrometer (AIS), developed at the Jet Propulsion Laboratory. This instrument acquired data in 128 spectral bands in the range of 1200-2400 nm with a field-of-view of 3.7 degrees (Vane & Goetz, 1985). In 1987 NASA began data acquisition with an improved version of AIS called the Airborne Visible/Infrared Imaging Spectrometer (AVIRIS; see Macenka & Chrisp, 1987). This scanner makes possible the simultaneous collection of images in 224 contiguous bands resulting in a complete reflectance spectrum for each 20*20 m. picture element (pixel) in the 400 to 2500nm region with a sampling interval of 10 nm (Goetz et al., 1985; Vane & Goetz, 1988; Porter & Enmark, 1987). The field-of-view of the AVIRIS scanner is 30 degrees resulting in a ground field-of-view of 10.5 km. The signal-to-noise ratio is 100:1 at 700nm and 50:1 at 2200nm. The value of this scanner lies in its ability to acquire a complete reflectance spectrum for each pixel. Many surface materials have diagnostic absorption features that are 20-40nm in width (Hunt, 1979). Therefore, spectral imaging systems which have 10nm wide bands can produce data with sufficient resolution for resolving these features and subsequent direct identification of those materials (Goetz, 1991). On the contrary, Landsat scanners, which have band widths between 100 and 200nm cannot resolve these spectral features. Analysis of high spectral resolution imagery for mineral identification involves three steps: (1) the pre-processing of the data to convert raw spectra into reflectance spectra corrected for atmospheric influences, (2) extraction of absorption features characterizing surface materials of interest, and (3) evaluating for each pixel whether the absorption feature is present or absent at the wavelength (Okada et al., 1991).

This paper shows the potential use of indicator kriging based techniques for image classification (the third processing step mentioned above) of remotely sensed imagery in general and high spectral resolution data in particular. AVIRIS data from the Cuprite mining district were used to detect occurrences of kaolinite and alunite based on their spectral characteristics. Four bands defining the key absorption features from these minerals are subsequently used as input

for classification and the results are compared with those derived from an indicator kriging based technique. To evaluate the results, synthetic measurements of shape are used and classification results are compared with field evidence deduced from local geological studies.

GEOLOGY AND SPECTRAL CHARACTERISTICS OF SURFACE MATERIALS

The area of study, the Cuprite mining district (figure 1) is situated in western Nevada and contains both hydrothermally altered and unaltered rocks which are well exposed and nearly devoid of vegetation. The mining district straddles the US highway 95 approximately 30 km south of Goldfield. Exposures of hydrothermally altered rocks about 12 km2 in extent which include minor sulphur, silica, and precious metals which have been exploited (Albers & Stewart, 1972). The eastern half of the district, which is discussed here, is an area of extensive hydrothermal alteration within a sequence of rhyolitic welded ash flow and air fall tuffs. The altered rocks are divided into three mappable units: silicified rocks, opalized rocks, and argillized rocks. Silicified rocks, containing abundant hydrothermal quartz, form a large irregular patch extending from the middle to the south end of the area. Opalized rocks contain abundant opal and as much as 30% alunite and kaolinite. Locally, an interval of soft, poorly exposed material mapped as argillized rock separates fresh rock from opalized rock. In the argillized rocks, plagioclase is altered to kaolinite, and glass is altered to opal and varying amounts of montmorrillonite and kaolinite. The general geology of the Cuprite mining district is treated in more detail in Abrams et al. (1977). The AVIRIS data used in this study were acquired on 29 september 1989 at 11:25 AM (local time).

Evaluating a 224 channel spectrum of 5x5 pixel area of the Stonewall Playa (denoted by A in figure 1) shows that the major features are the broad atmospheric water bands centered at 1400 and 1900nm and the solar irradiance curve which exhibits a rapid falloff toward long wavelengths. A shortcut to modelling the atmospheric and insolation effects can be made if the data are normalized to an area in the image having little or no topographic relief and uniform, known spectral reflectance characteristics. The flat-field area chosen for the correction should have a high albedo to avoid introducing noise and sacrificing the signal-to-noise ratio. This normalization procedure, known as the flat-field-correction, has been applied to the data by dividing the original DN values by the corresponding value in the Stonewall Playa spectrum. Spectral features in the surface material become more apparent in the normalized spectrum because of the removal of systematic effects makes it possible to display the data at their full radiometric resolution. Other correction techniques are the log-residual correction (Green & Graig, 1985) and a correction technique using the LOWTRAN 7 (Kneizys et al., 1988) atmospheric model (see Rast et al., 1991 for a complete review).

The potential use of Imaging Spectrometry for mapping of hydrothermal alteration minerals in the Cuprite mining district has been shown by many workers (e.g. Goetz et al., 1985; Vane, 1987).

Figure 2 shows normalized spectra from areas B, C and D in figure 1. Area B is known as Kaolinite Hill for its extensive and well exposed deposit of the clay mineral kaolinite. The wavelength positions of the double OH absorption features

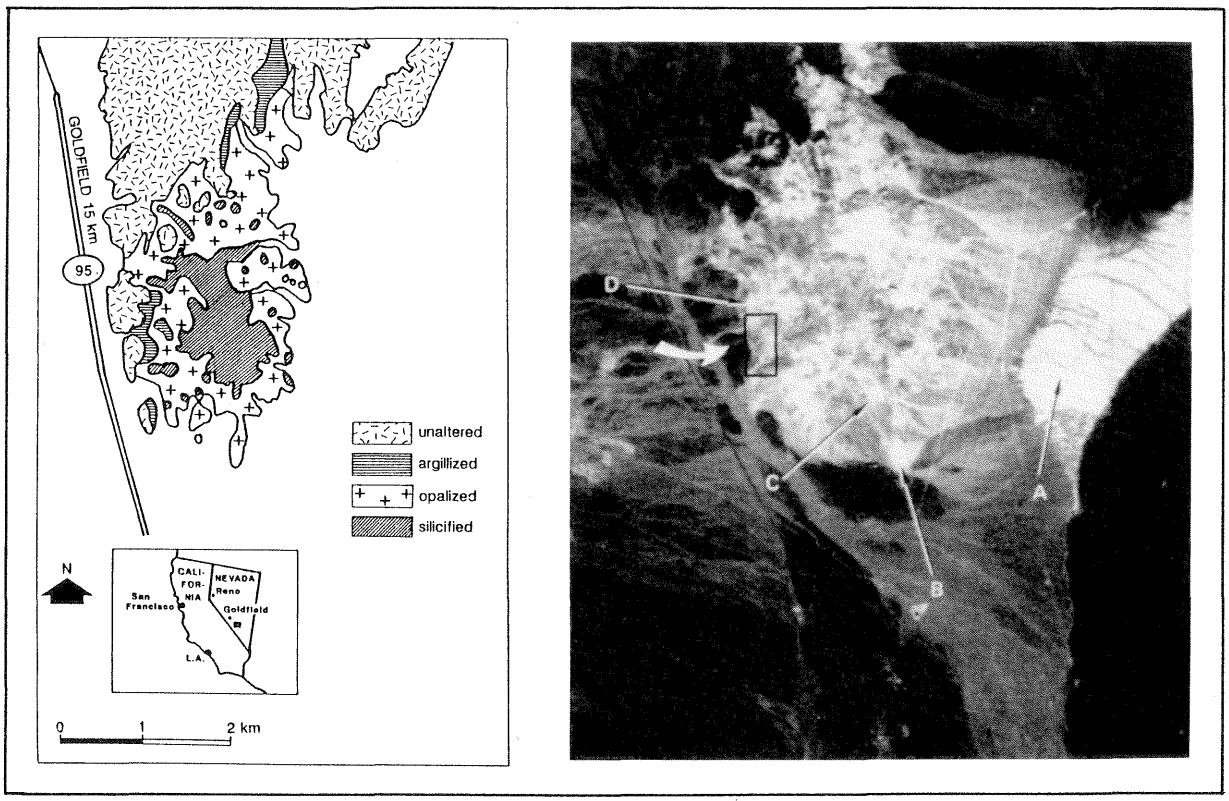

figure 1: AVIRIS image of the Cuprite mining district (right) in band centered at 1014nm (A=Stonewall Playa; B=Kaolinite Hill; C=Alunite occurrence; D=Buddingtonite occurrence). The box indicates the area selected for classification. The map (left) is a display of the alteration zones after Ashley (1977).

at 2160 and 2200nm which is seen in laboratory spectra (Hunt & Salisbury, 1970; VanderMarel & Beutelspacher, 1976) and resolved in the AVIRIS spectrum, was the main criterium used for positive identification. Furthermore, the characteristic asymmetric shape of the spectrum towards long wavelengths is well seen. Other clay minerals which are difficult to distinguish from kaolinite visually are alunite and buddingtonite. Alunite occurs widely throughout the Cuprite mining area while buddingtonite has been observed at few locations at the site. The occurrence of buddingtonite was discovered through the analysis of AIS spectra (Goetz & Srivastava, 1985). An absorption feature at 2020nm and a vibrational absorption feature due to NH4 (Krohn & Altaner, 1987) at 2110nm are the main diagnostic features distinguishing buddingtonite spectrally from other clay minerals. Alunite is characterized by absorption features at 2160 and 2200nm due to OH frequency stretching (Hunt et al., 1971) and a nearly symmetrical shape in the 2080-2280nm region.

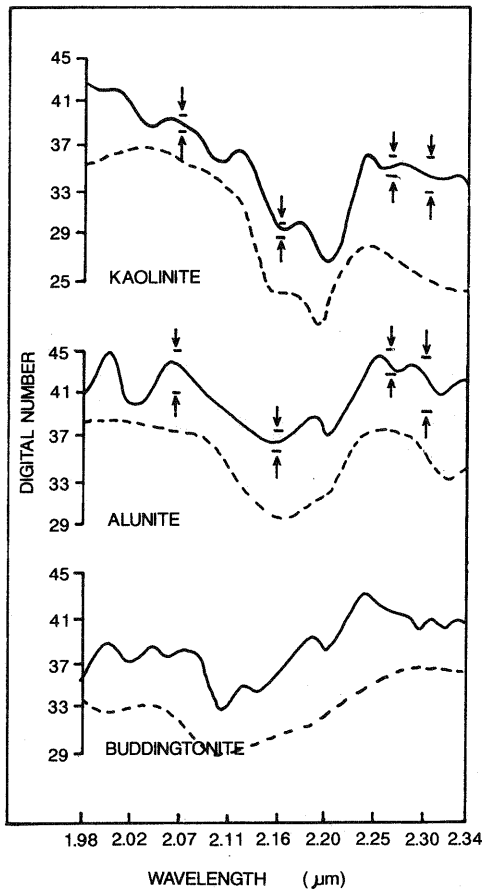

Figure 2: Mineral spectra for Kaolinite (top), Alunite (middle) and Buddingtonite (bottom) derived from AVIRIS imagery using a 5x5 pixel area at locations indicated by B, C, and D respectively in figure 1. Dotted curves represent laboratory spectra of the investigated minerals. Arrows enclose the ranges used for indicator classification in the four bands used.

METHODS FOR SUPERVISED CLASSIFICATION

After establishing mineral spectra, the next processing step is to apply classification rules to the image data to investigate spatial distribution of mineral occurrences. As discussed previously, conventional classification methods selecting bands on the shoulders and centre of absorption features will be used and compared to an indicator kriging based method selecting the same bands.

Conventional Classification Methods

The processing strategy for information extraction from multiple datasets usually involves image classification. Classification techniques are based on computer assisted recognition of surface materials from their characteristic spectral properties in various wavelength bands. During investigation of imagery and during field check, areas known to represent the outcrop of a mineral or rock of interest are being selected as training areas. For each band which is used in the classification the spectral range for each class is estimated from the training pixels. Combining the information for various bands results in an N-dimensional histogram (the feature space) from which all classes can be separated according to their spectral response. The next step is to give the computer a set of rules to classify all pixels in an image by comparing their spectral response in various bands with those of the training pixels. The simplest method of doing so is box classification by which the two dimensional feature spaces are divided into rectangular boxes. The boundaries of the boxes representing the spectral ranges of DN values for the two bands within known area of the surface categories. Box classification compares all unknown pixels with the boxes; if they fall within one box they are assigned to the relevant class, if they fall in no box they remain unclassified. An important limitation of this method is that natural earth materials generally plot as ellipsoids in N-dimensional feature spaces, and boxes are only a crude representation of ellipses (figure 3b).

A more sophisticated set of rules is provided by the K-nearest neighbour analysis which employs the statistics of the data from training areas. This method, first identifies the mean for each class used and secondly assigns the unknown pixel to the class with the closest mean. A userdefined search radius is adopted; if this distance is exceeded the pixel will remain unclassified (figure 3a).

A refinement to this method is the maximum likelihood classification method which also uses the variance of the training samples. If DN values within the training areas are assumed to be normal distributed for each band, histograms can be considered to be bell-shaped. Dependent on the variance, the further a DN is from the mean, the less the probability is that it represents the class. In a two dimensional feature space, DN values from training pixels form a elliptical cloud which can be contoured to show the decrease of the probability from the mean value. The plot of DN for any unknown pixel can then be assessed in this probabilistic context by calculating the likelihood of the pixel belonging to each of the predefined classes. The unknown pixel is assigned to the class for which the likelihood (=probability) is maximized (figure 3c). The main disadvantages of these conventional classification methods is that training pixels have to be selected which is often a tedious task. Furthermore, none of the methods discussed gives information on the reliability of the classification results and only maximum likelihood classification defines the probability of a pixel belonging to a class.

Analysis of high spectral resolution imagery uses spectral bands on the shoulders and centre of an absorption feature to deduce maps for the wavelength position, width, depth, symmetry, and Hull quotient of absorption features to investigate the spatial distribution of surface mineralogy (figure 3d).

The Indicator Kriging Method

The new classification method, the indicator kriging based method, allows for multispectral classification without prior knowledge of ground truth. Instead of using training pixels to define spectral ranges of classes of interest, this method directly employs the mineral spectra derived using AVIRIS or other type of scanner data.

Indicator kriging is one of the non-parametric geostatistical techniques which discretizes the histogram into several classes and carries out interpolation separately for every class (Fytas et al., 1989; Dagbert, 1990). The principal difference between ordinary kriging and indicator kriging is that indicator kriging works on (0,1) transformed data according to several threshold levels. Therefore the final result of indicator kriging is a set of probabilities that a block exceeds a specific set of cut-off values. In general, five steps are required to carry out estimation using indicator kriging (Fytas et al., 1989): (1) construct histograms for input data, (2) choose threshold values from the histograms, (3) transform data values into 0,1 values (1 if they are below the threshold and 0 if they are above the threshold), (4) develop variogram models for all cut-offs, and (5) perform kriging on the 0,1 transformed data repeating the process for every threshold to get as an end product a cumulative probability. Indicator kriging is based on the theory of regionalized variables (Matheron, 1971) in which a variable is distributed in space. Local estimation tries to find the best estimator of the mean value of a regionalized variable over a limited domain whereas global estimation considers larger distances thus, sometimes, engulfing various heterogeneous mineralizations (Journel & Huijbregts, 1978, p. 304). Assuming that the regionalized variable has values $Z_i = Z(x_i)$ which represent the value at point x_i, the expectation (E) for a second order stationary variable is then given by:

$$E\{Z(X)\} = m \qquad (1)$$

where m is a constant which is generally unknown. The variance of the difference between the value of the variable at two points Z(x) and Z(x+h) a distance h apart is described using the variogram ($2\gamma(h)$) and semi-variogram ($\gamma(h)$) or the covariance function (C(h)) given by:

$$E\{[Z(x+h) - Z(x)]^2\} = 2\gamma(h) \qquad (2)$$

and

$$E[Z(x+h)\,Z(x)] - m^2 = C(h) \qquad (3)$$

respectively. A kriged estimate Z_k^* is a weighted linear combination of n values of the regionalized variable given by:

$$Z_k^* = \sum_{i=1}^{n} \lambda_i Z_i \qquad (4)$$

where Z_i is the observed value of the variable at sample point i and λ_i is the weight attached to the value at sample point i. Weights are calculated so that the average error of the estimate over a great number of similar estimations (i.e. observed value minus estimated value) is minimised and to ensure that the estimate is unbiased. The last criterion is satisfied by requiring the weights to sum up to one, resulting in:

$$E\{Z_k^*\} = m \sum_{i=1}^{n} \lambda_i = m = E\{Z_v\} \qquad (5)$$

which yields:

$$E\{Z_v - Z_k^*\} = 0 \qquad (6)$$

The first criterion, minimising the error variance $E\{Z_v - Z_k^*\}$ can be expanded as follows:

$$E\{[Z_v - Z_k^*]^2\} = E\{Z_v^2\} - 2E\{Z_v Z_k^*\} + E\{Z_k^{*2}\} \qquad (7)$$

Following David (1977, p. 243) and Journel & Huijbregts (1978, p. 306) the minimum estimation variance or kriging variance can be written as:

$$\sigma^2_k = C(V,V) + \mu - \sum_{i=1}^{n} \lambda_i C(V_i,V) \qquad (8)$$

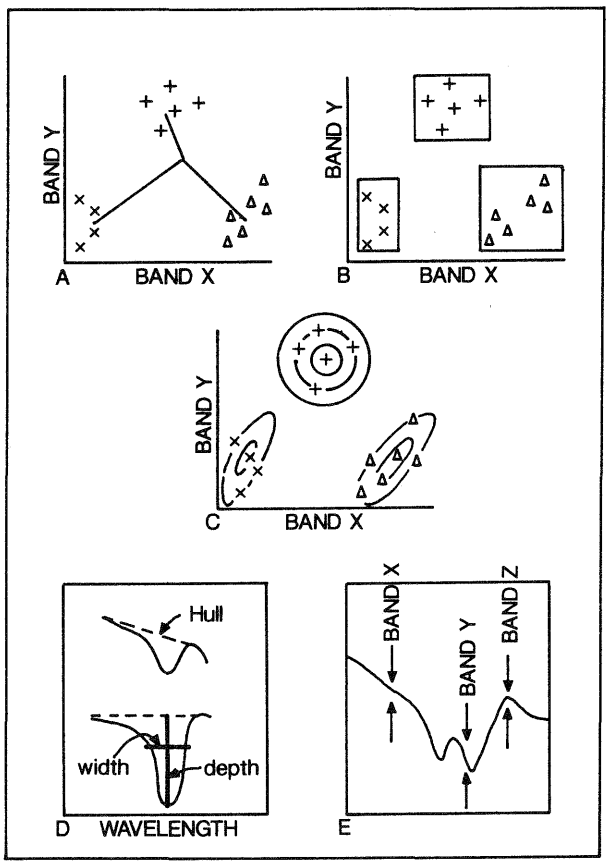

Figure 3: Schematic representation of different classification methods: (A) K-Nearest Neighbour analysis, (B) Box classification, (C) Maximum likelihood decision rules, (D) absorption parameters used for the analysis of AVIRIS data, and (E) indicator kriging definition of bands and upper and lower limits (see text for explanation).

or expressed in terms of the semi-variance function $\gamma(h)$ as:

$$\sigma^2_k = \Sigma_i \lambda_i \gamma(v_i,V) + \mu - \gamma(V,V) \qquad (9)$$

where $C(v_i,V)$ represents the covariance between any point in the block, V, and sample v_i ($\gamma(v_i,V)$ is the corresponding semi-variance), C(V,V) is the average covariance of samples within block area V (with the corresponding semi-variance value $\gamma(V,V)$), and μ is the Lagrange multiplier added to ensure a statistically optimal result.

In practice, the computations of block values is carried out through a discrete summation. The area of the block is represented by a group of points regularly disposed over the area. Precision increases with the number of points within the area. In practice geostatistical analysis starts by calculating a semivariogram describing the spatial variability of the variable to be estimated. This semivariogram is used to derive the weights assigned to each sample point during the kriging interpolation resulting in an estimate and error variance for all block areas.

Classification using the indicator kriging approach starts by defining the spectral bands that contain "key information" on the spectral response of a certain ground class of interest. This step is done by extracting absorption features characterizing a mineral of interest from field spectral analysis or laboratory measurements. Bands on the shoulders of the absorption feature and bands on the centre of the feature are subsequently used for further analysis. This first step requires information on the spectral characteristics of certain minerals and not necessary on field geology which is obligatory for proper selection of training areas. The next step is to define the spectral range in each band by means of setting upper and lower limits for the DN values in those spectral bands. Figure 3e shows the diagnostic absorption feature for kaolinite which can be mapped using two bands defining the shoulders and one band marking the centre of the feature. Upper and lower limits in each bands are indicated by the area enclosed in between the arrows. For all of these limits the data are being transformed into 0 and 1 values; 1 if they are below the threshold and 0 if they are above the threshold. The result are two binary (0,1) maps for each spectral band used in the classification; one for the upper limit and one for the lower limit. Subsequently, the binary maps are interpolated using the ordinary kriging procedure described above. By interpolating the 0,1 map for the upper limit we gain a map representing the probability that the value of a block lies below the indicated upper limit. The interpolation for the lower limit results in a map representing the probability that the block value lies above the lower limit. Combining these we calculate the probability that the block DN value is higher than the lower limit and smaller than the upper limit (e.g. the probability of a block having a spectral DN value in between the predefined range corresponding to the spectral response of the mineral of interest. The size of the blocks to produce output can be defined by the user and is not necessary of the same size as the input pixel size. This provides a means of extrapolating to areas smaller than the pixel size. Repeating this procedure for all key bands results in a set of probability maps (one for each band) which can be integrated by calculating the joint probability which is a measure for the likeliness that a pixel belongs to a certain class. This image is used as input for the classification. By setting tolerances on the minimum probability acquired for each class, pixels can be classified with a predefined accuracy.

RESULTS

Different classification methods have been applied to a small (50x20 pixels) area located in the northwestern part of the image (figure 1). This area was chosen for its known occurrence of both kaolinite and alunite rich deposits. Therefore classification focused on these two minerals using bands centered at 2060, 2160, 2260 and 2300nm. From the mineral spectra derived from AVIRIS it can be shown that both alunite and kaolinite have an absorption feature at 2160nm which differs significantly in depth. Furthermore, the shape of the spectra over the spectral range 2060-2300nm is different (figure 2).

Classification results of conventional methods are shown in figure 4. Training samples were chosen at sites indicated by Kaolinite Hill and Alunite in figure 1. For the indicator

Figure 4: Classification results for ground classes Kaolinite and Alunite using (A) Box classification, (B) K-Nearest neighbour analysis, (C) maximum likelihood decision rules, (D) indicator kriging using probability values greater than 0.5, and (E) indicator kriging using probability values greater than 0.

classification method the threshold values used in all four bands are shown in figure 2. Indicator variograms are well defined at low cutoffs but tend to become conspicuous at high cutoffs. These variograms are a measure for the variability in the dataset and are used in the interpolation procedure to derive the kriging weights. Indicator kriging derived probability maps for alunite and kaolinite are shown in figure 5. These have been transformed into classified images by using all probabilities greater than zero (referred to as the indicator maximum result) and by using all probabilities greater than 0.5 (referred to as the indicator minimum results). The classified images for the indicator kriging based method are shown in figure 4.

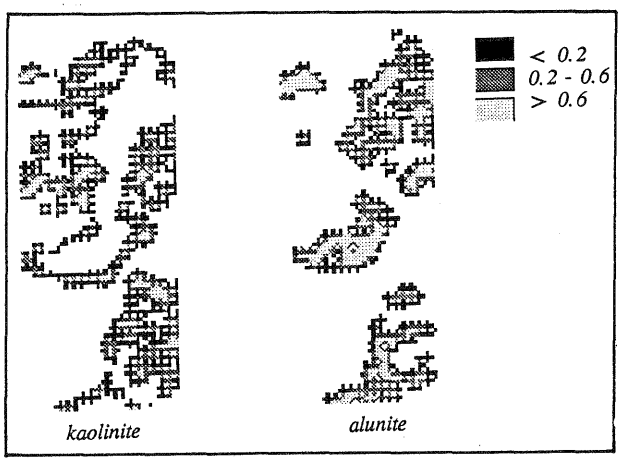

Figure 5: Probability that a pixel belongs to class kaolinite (left) or alunite (right). By setting tolerances on the probability values, pixels can be classified. From these images, the final classification was deduced by setting tolerances on the probability (e.g. $P > 0.5$ for indicator minimum and $P > 0$ for indicator maximum classification).

Equations 8 and 9 reveal an important feature of kriging: the estimation variances depend on the semivariogram and, through it, on the configuration of observation points in relation to the block to be estimated and on the distances among them. They are independent of the observed values themselves, thus if a semivariogram is known then kriging variances for any sampling scheme can be determined prior to sampling (McBratney et al., 1981). By means of a similar procedure an assessment of the reliability of the output results for different block sizes can be made. Provided the variogram is known and the spacing and size of the input data (in this case 20x20 m pixels) for each output block geometry the maximum error can be calculated (McBratney et al., 1981). The maximum error for each upper and lower limits in each band has been evaluated for the class alunite (table I). Input data are on 20x20 m regular grid whereas output has been produced on grids of 1x1, 10x10, 20x20, 40x40, 80x80, and 100x100 m. An exponential decrease of error is clearly seen with increasing blocksize although the difference for block sizes exceeding the pixel size is insignificant. For this study, output was produced on a 10x10 m. grid yielding a average error of 18%.

EVALUATION OF RESULTS

The classification results have been evaluated by comparing the classified images with the field information from Albers & Stewart (1972) and Ashley (1977) and secondly by quantifying the visual aspects of the classes using synthetic measurements of shape. Tables IIa and IIb show the results of the comparison between classification and field evidence for the distribution of kaolinite and alunite, respectively. Four different combinations can occur (table IIa+b): (1) in both the classified image and the field geologic map the pixel is classified as mineral (column 1), (2) only in the field the mineral occurrence is detected not in the classified image (column 2), (3) only in the classified image the pixel is assigned to the class representing the mineral
to occur although no evidence was found in the field geologic map (column 3), and (4) the pixel in the image and in the field geologic map were not considered to belong to the class of the mineral investigated. The classification results for kaolinite are in general poor although the indicator kriging technique adopting a probability of zero scores relatively good with respect to the conventional classification methods. For the class alunite surprisingly good results were obtained by the maximum likelihood decision rules and by the indicator kriging technique using all probability values greater than zero.
Instead of counting correctly classified pixels, one can also look at the visual aspects of classified images to evaluate classification results. Some aspects with respect to this are the roundness of the clusters and the number of holes in them. Mathematical morphology (Serra, 1982) quantifies the geometrical structure and texture of an object by introducing the concept of the structuring element. This element interacts with the object under study, modifying its shape and reducing it to a caricature which is more expressive than the initial phenomenon. Basic transformations of binary patterns are erosion, opening and closing (Fabbri, 1984) from which

table I: Kriging standard deviation for estimation of class alunite in four bands used.

block size	band 2060nm		band 2160nm		band 2260nm		band 2300nm	
	lower	upper	lower	upper	lower	upper	lower	upper
1 x 1	0.15	0.10	0.24	0.25	0.22	0.16	0.23	0.24
10 x 10	0.09	0.06	0.15	0.20	0.10	0.10	0.20	0.17
20 x 20	0.07	0.06	0.10	0.20	0.10	0.10	0.10	0.10
40 x 40	0.06	0.05	0.10	0.10	0.09	0.08	0.09	0.10
80 x 80	0.06	0.04	0.08	0.09	0.06	0.06	0.09	0.09
100 x 100	0.06	0.04	0.01	0.02	0.05	0.01	0.08	0.07

table IIa: Kaolinite occurrence versus predicted.

	both	in field	in image	none
indicator kriging				
min: P > 0.5	5.7%	16.3%	0.4%	77.6%
max: P > 0.0	18.2%	3.8%	7.2%	70.8%
box classification	3.1%	18.9%	7.6%	70.4%
K-nearest neighbour	0.9%	21.1%	4.2%	73.8%
Maximum likelihood	----	-----	----	----

table IIb: Alunite occurrence versus predicted.

	both	in field	in image	none
indicator kriging				
min: P > 0.5	11.3%	13.3%	0.1%	75.3%
max: P > 0.0	21.0%	3.4%	2.2%	73.4%
box classification	12.3%	12.2%	1.1%	74.4%
K-nearest neighbour	12.8%	11.7%	0.9%	74.6%
Maximum likelihood	20.1%	4.5%	4.8%	70.6%

synthetic measurements of shape are derived quantifying the visual aspects of a class (Fabbri et al., 1990). In this study, measurements used were (1) the index of morphologic compactness, (2) the connectivity number, and (3) the boundary density (Durand & Flouzat, 1985).

The index of morphologic compactness (IC(c)) is an indication for the roundness of particles in a class. The index varies from 0 to 1 where IC(c)=1 is a class composed of entities with rounded edges and IC(c)=0 is a class composed of entities with a blocky character.

The connectivity number (NC(c)) defines the number of particles in class c minus the number of holes in them. The higher the number of entities, the greater the disseminated aspect of the class.

The boundary density (DF(c)) represents application to a given class of the shape coefficient for isolated objects, and provides information on the physiognomy of edges in that class.

The results of the calculation of synthetic measurements of shape are shown in table III.

The morphological compactness of classes alunite and kaolinite in the box classified image and the K-nearest neighbour image are low giving them a blocky aspect. Maximum likelihood classification yields better results, however, the indicator kriging classified images score best

table III: Morphological characteristics of classification results.

BOX CL.		MAX. LIK.		K-NEAR		INDIC.MIN		INDIC.MAX		
alun	kaol	alun	kaol	alun	kaol	alun	kaol	alun	kaol	
.17	.07	.38	++	.17	.01	.50	.20	.62	.39	IC(c)
.84	.93	.68	++	.87	.98	.66	.82	.57	.73	DF(c)
20	45	4	++	16	32	28	49	9	16	NC(c)

with this respect. The connectivity number of all methods is high, especially for the class kaolinite, although maximum likelihood classification and the indicator kriging based methods perform best with this respect. The boundary density for the indicator kriging based methods is significantly lower than for the conventional classification techniques, thus indicating less isolated objects.

CONCLUSIONS

Direct identification of earth surface materials on the basis of their unique spectral reflectance features is now possible using imaging spectrometry (e.g. AVIRIS) in comparison with laboratory spectra. New image processing and analysis methods have to be developed in order to cope with the large amount of data available. Indicator kriging techniques as classification routines for image analysis allows for direct use of spectral information without prior knowledge of the geology of the area. A major advantage of this new technique is that it gives access to the reliability of the results and that areas smaller than the pixel size can be classified. In terms of visual aspects of classes and in terms of correctness of the classification, the new method performs better than the conventional methods.

REFERENCES

Abrams, M.J., Ashley, R.P., Rowan, L.C., Goetz, A.F.H. and Kahle, A.B. (1977) "Use of imaging in the 400-2360nm spectral region for alteration mapping in the Cuprite mining district, Nevada", US Geol. Survey Open file Report 77-585, pp. 1-19.

Albers, J.P. and Stewart, J.H. (1972) "Geology and mineral deposits of Esmeralda County, Nevada", Nevada Bur. Mines and Geology Bull. 78, pp. 1-80.

Ashley, R.P. (1977). "Geologic map and alteration map, Cuprite mining district, Nevada.

Dagbert, M. (1990) "Nested indicator approach for ore reserve estimation in highly variable mineralization", Paper 101, 92nd Annual General meeting of the Canadian institute of Mining and Metallurgy, may 6-16, Ottawa, Canada.

DAVID, M. 1977.: Geostatistical ore reserve estimation, Elsevier, New York: 364 pp.

Durand, M.A. and Flouzat, G. (1985) "Quantification de l'aspect visuel des images classees", Photo interpretation 3, fascicule 5, 47-51.

Fabbri, A.G. (1984) Image processing of geologic data, Van Nostrand Reinhold publishers, New York.

Fabbri, A.G., Kushigbor, C.A., Valenzuela, C.R. and van der Meer, F.D. (1990) "Automated strategies for geometric characterization in geological remote sensing", 4th International Conference of Geoscience information (GEOINFO-4), 24-29 june 1990, Ottawa, Canada.

Fytas, K., Chaouai, N.E. and Lavigne, M. (1989) "Indicator kriging performance in gold deposit evaluation", Paper, 58, 91th Annual General meeting of the Canadian Institute of Mining and Metallurgy, 30 april, 3 may, Quebec City, Quebec, Canada.

Goetz, A.F.H. (1991) "Imaging Spectrometry for studying Earth, Air, Fire and Water", EARSel Advances in Remote Sensing 1, 3-15.

Goetz, A.F.H. and Srivastava, V. (1985) "Mineralogical mapping in the Cuprite mining district, Nevada", in: G. Vane and A.F.H. Goetz (eds.), Proceedings of the Airborne Imaging Spectrometer Data analysis Workshop, JPL Publication 85-41, Pasadena, California, pp. 22-31.

Goetz, A.F.H. and Rowan, L.C. (1981) "Geologic remote sensing", Science 211, 781-791.

Goetz, A.F.H., Vane, G., Solomon, J.E. and Rock, B.N. (1985) "Imaging spectrometry for earth remote sensing", Science 228, 1147-1153.

Green, A.A. and Graig, M.D. (1985) "Analysis of aircraft Spectrometer data with logarithmic residuals" in: G. Vane and A.F.H. Goetz (eds.), Proceedings of the Airborne Imaging Spectrometer Workshop, JPL Publication 85-41, Pasadena, California, pp. 111-119.

Hunt, G.R. (1977) "Spectral signatures of particulate minerals in the visible and near infrared", Geophysics 42, 501-513.

Hunt, G.R. (1979), "Near Infrared (1.3-2.4 m) Spectra of alteration minerals; potential for use in remote sensing", Geophysics 44, 1974-1986.

Hunt, G.R. and Salisbury, J.W. (1970) "Visible and near-infrared spectra of minerals and rocks I: silicate minerals", Modern geology 1, 283-300.

Hunt, G.R., Salisbury, J.W. and Lenhoff, C.J. (1971) "Visible and near infrared spectra of minerals and rocks IV: Sulfides and sulfates", Modern Geology 3, 1-14.

JOURNEL, A.G. & HUIJBREGTS, G.H. 1978.: Mining Geostatistics, Academic press, New York, 600 pp.

Kneizys, F.X., Anderson, G.P., Shettle, E.P., Gallery, W.O., Abreu, L.W., Selby, J.E.A., Cetwynd, J.H. and Clough, S.A. (1988) "Users guide to LOWTRAN 7", Air Force Geophysics Laboratory, Hanscom AFB, Massachusetts AFGL-TR-88-0177.

Krohn, M.D. and Altaner, S.P. (1987) "Near Infrared detection of ammonium minerals", Geophysics 52, 924-930.

Macenka, S.A. and Chrisp, M.P. (1987) "Airborne Visible/Infrared Imaging Spectrometer, Design and Performance", in: G. Vane (ed.), Airborne Visible/Infrared Imaging Spectrometer AVIRIS (A description of the sensor, ground data processing facility, Laboratory Calibration, and first results, JPL Publication 87-38, Pasadena, California, pp. 89-97.

MATHERON, G. 1971.: The theory of regionalized variables and its applications, Centre de Geostatistique, Fontainebleau, France: 211 pp.

McBratney, A.B., Webster, R. and Burgess, T.M. (1981) "The design of optimal sampling schemes for local estimation and mapping of regionalized variables I: theory and method", Computer & Geosciences 7, 331-334.

Okada, K., Ohnuma, T. and Watanabe, H. (1991) "Geologic mapping of Keping uplift, Northwestern margin of Tarim basin based on absorption features using hyper-multispectral image data", Second annual JPL airborne Geoscience Workshop: AVIRIS, may 20-21, Pasadena, California.

Porter, W.M. and Enmark, H.T. (1987) "A system overview of the Airborne Visible/Infrared Imaging Spectrometer (AVIRIS)", proceedings of the 31th annual International Technical Symposium, 16-21 august 1987, Soc. of Photooptical Instrumentation Engineers V834, 22-31.

Rast, M., Hook, S.J., Elvidge, C.D. and Alley, R.E. (1991) "An evaluation of techniques for the extraction of mineral absorption features from High Spectral Resolution Remote Sensing data", Photogrammetric Engineering & Remote Sensing 57, 1303-1309.

Serra, J. (1982) Image analysis and Mathematical Morphology, Academic Press, New York.

VanderMarel, H.W. and Beutelspacher, H. (1976) Atlas of infrared spectroscopy of clay minerals and their admixtures, Elsevier, New York.

Vane, G. (1987) "First results from the Airborne Visible/Infrared Imaging Spectrometer (AVIRIS)", in: G. Vane (ed.), Airborne Visible/Infrared Imaging Spectrometer AVIRIS (A description of the sensor, ground data processing facility, Laboratory Calibration, and first results, JPL Publication 87-38, Pasadena, California, pp. 89-97.

Vane, G. and Goetz, A.F.H. (1985) "Introduction for the proceedings of the Airborne Imaging Spectrometer (AIS) Data analysis workshop", in: G. Vane & A.F.H. Goetz (eds.), Proceedings of the Airborne Imaging Spectrometer (AIS) data analysis workshop, JPL Publication 85-41, Pasadena, California.

Vane, G. and Goetz, A.F.H. (1988) "Terrestrial Imaging Spectroscopy", Remote sensing of environment 24, 1-29.